

SrAl₂O₄:Eu²⁺, Dy³⁺: SYNTHESIS, LUMINESCENCE, PROPERTIES, AND APPLICATION

Mihail Nazarov

Institute of Applied Physics, Academiei str. 5, Chisinau, MD 2028 Republic of Moldova
E-mail: mvnazarov@mail.ru

(Received July 6, 2020)

DOI: 10.5281/zenodo.4118682

CZU:535.37+544

Abstract

Single-phase SrAl₂O₄:Eu²⁺ and multiphase {SrAl₂O₄+Sr₄Al₁₄O₂₅}:Eu²⁺ phosphors, as well as those codoped additionally with Dy³⁺, are prepared by solid state reaction and combustion synthesis. The codoping of SrAl₂O₄:Eu²⁺ with Dy³⁺ leads to an increase in the afterglow duration from a few minutes up to many hours and makes the afterglow much brighter, which is important in some applications. It is shown that the emission band of the phosphors can be shifted from green to blue-green spectral range by changing the synthesis method. Composite color cathodoluminescence and photoluminescent analysis are applied to control the synthesis process. The presence of different emission centers and their distribution in the studied phosphors is shown. Some of their numerous applications, such as display devices, painting, and biological applications, are shown.

Keywords: SrAl₂O₄:Eu,Dy, Sr₄Al₁₄O₂₅:Eu,Dy, color cathodoluminescence, photoluminescence.

Rezumat

Luminoforii monofazici SrAl₂O₄:Eu²⁺ și luminoforii multifazici {SrAl₂O₄+Sr₄Al₁₄O₂₅}:Eu²⁺, precum și cei dopați suplimentar cu Dy³⁺, au fost obținuți prin reacție în fază solidă și sinteză prin combustie. Datorită dopării suplimentare a SrAl₂O₄:Eu²⁺ cu Dy³⁺, postluminescența a crescut de la câteva minute la multe ore și a devenit mult mai luminoasă, ceea ce este important în unele aplicații. Se arată că banda de emisie a luminoforilor poate fi deplasată de la spectrul verde la cel albastru-verde prin schimbarea metodei de sinteză. Pentru a controla procesul de sinteză, s-au aplicat catodoluminescența color și analiza fotoluminescenței. Se demonstrează prezența diferitelor centre de radiație și distribuția lor în luminoforii investigați. Sunt prezentate unele dintre numeroasele domenii de aplicații, cum ar fi, dispozitive de afișare, pictură și biologie.

Cuvinte cheie: SrAl₂O₄:Eu,Dy, Sr₄Al₁₄O₂₅:Eu,Dy, catodoluminescență color, fotoluminescență.

1. Introduction

Alkali earth aluminates phosphors doped with rare-earth ions (especially with Eu^{2+}) are functional inorganic materials with strong luminescence covering a wide spectral range: from blue to red regions of the visible spectrum. These materials have recently attracted considerable attention, which is determined by their numerous applications, such as display devices, signage, medical application, emergency rescue guidance system, storage devices, arts and craft, fluorescent lamps, plasma display panels, and many others. Additionally, these systems have been regarded as excellent long-persistence phosphors based on their highly efficient luminescence centers and possibility of emitting light for a long time after the excitation has ended. Since the mid 1990s, a completely new generation of persistent luminescent phosphors has been developed and entered into commercial market. In recent years, strontium aluminates, especially SrAl_2O_4 and $\text{Sr}_4\text{Al}_{14}\text{O}_{25}$ doped with rare-earth ions, have been regarded as promising candidates due to their excellent luminescence properties. Several methods were initially used for their synthesis, such as conventional solid state reaction (SSR), sol-gel method, combustion and microwave heating synthesis. The most important results regarding this system are summarized in recent publications and reviews [1–14]. Despite the fact that intensive studies of these materials in the last two decades led to the understanding of the key aspects of their optical properties, some new challenging results appear every year.

In some cases, especially in phosphor converted light-emitting diode (pc-LED) applications, it is necessary to tune the color of emission. In the present study, multiphase Eu-doped persistent phosphors $\{\text{SrAl}_2\text{O}_4+\text{Sr}_4\text{Al}_{14}\text{O}_{25}\}$ were synthesized. The synthesis process was controlled using color cathodoluminescence (CCL) express analysis and proved by direct photoluminescence (PL) measurements. The emission of the synthesized phosphors is highly efficient and its wavelength depends on the relative concentration of $\text{SrAl}_2\text{O}_4/\text{Sr}_4\text{Al}_{14}\text{O}_{25}$ phases. In SrAl_2O_4 host lattice, the main emission band of Eu^{2+} ions is centered near 520 nm, while that of $\text{Sr}_4\text{Al}_{14}\text{O}_{25}$ is centered at 490 nm. Changing the synthesis method, we can shift the emission from green to blue-green spectral range. The $\{\text{SrAl}_2\text{O}_4+\text{Sr}_4\text{Al}_{14}\text{O}_{25}\}$ based phosphor was also codoped with Dy^{3+} ions, as they can further enhance the luminescence properties and prolong the afterglow of phosphor. The other goal of this research is to show the advantages of CCL-PL analysis in the study of the luminescent properties of strontium aluminate-based phosphors and show the phosphor applications.

2. Experimental

2.1. Specimen preparation procedure

Macro sized ($\sim 5 \mu\text{m}$) and nano sized ($\sim 130 \text{ nm}$) specimens of strontium aluminate were prepared by SSR and combustion methods (see Table 1).

Table 1. Indication of synthesized specimens.

Specimen designation	Material composition	Synthesis methods
SAED	{SrAl ₂ O ₄ +Sr ₄ Al ₁₄ O ₂₅ }:Eu ²⁺ ,Dy ³⁺	Solid state reaction
SAE	{SrAl ₂ O ₄ +Sr ₄ Al ₁₄ O ₂₅ }:Eu ²⁺	Solid state reaction
SA	{SrAl ₂ O ₄ +Sr ₄ Al ₁₄ O ₂₅ }	Solid state reaction
CSAE	SrAl ₂ O ₄ :Eu ²⁺	Combustion method
CSAED	SrAl ₂ O ₄ :Eu ²⁺ ,Dy ³⁺	Combustion method
CSA	SrAl ₂ O ₄	Combustion method

Solid state reaction method. The conventional SSR is mostly used for preparation of bulk phosphors. Strontium aluminate phosphor SrAl₂O₄ (SA), as well as that doped with Eu²⁺ (SAE) and codoped with Dy³⁺ (SAED), were prepared by the SSR approach using strontium carbonate (SrCO₃; Aldrich, 99.9 %), alumina (Al₂O₃), europium oxide (Eu₂O₃; Aldrich, 99.99 %), and dysprosium oxide (Dy₂O₃; Aldrich, 99.99 %) as the starting materials. A small amount (0.2 mol %) of H₃BO₃ was used as a flux. The raw powders were mixed according to the nominal composition of SrCO₃ and Al₂O₃ for the host lattice SrAl₂O₄. To activate this host with Eu²⁺ and Dy³⁺ ions, Eu₂O₃ and Dy₂O₃ were used. The concentration of Eu²⁺ ions and Dy³⁺ ions was optimized separately. An appropriate amount of the starting materials was weighted and mixed. First, the dry milling was used for 30 min; after that, a small amount of water was added in the wet-mixing machine for homogeneity of the mixed powders, and the milling was conducted for 30 min. The resulting slurry was dried at 150°C for 3 h to remove water. Once fully dried, the mixed white powder was placed into a small alumina crucible and then fired consecutively at 1100, 1150, 1200, 1250, and 1300°C for 2 h under a mild reducing atmosphere. The physical parameters, such as a heating rate of 10°C per minute, a cooling rate of 10°C per minute, and a heating time of 2 h, were the same for all specimens. The small alumina crucibles with powders were put in a big graphite crucible and then heated at a fixed temperature for 2 h. Graphite crucibles were used to create a reducing atmosphere and provide the complete reduction of Eu³⁺ to Eu²⁺. The mixing–milling process was used after calcination to provide a smaller particle size and a homogenous mixture. A set of SrAl₂O₄:Eu²⁺ crystals with different Eu²⁺ ions concentrations: 0.3, 0.5, 0.7 and 1 mol % (all mole percents are taken relative to Sr²⁺) were synthesized to study the effect of Eu²⁺ activation. The next series of SrAl₂O₄:Eu²⁺,Dy³⁺ crystals with different Dy³⁺ ions concentrations: 1 mol, 2.5, 5, and 10 mol % were also prepared. The powder specimens with optimized dopant concentrations (0.7 mol % Eu²⁺ and 5 mol % Dy³⁺) were studied in this work. The specimens were prepared in two syntheses (#1 and #2), which were carried out under similar conditions in different time to verify the reproducibility of results.

Combustion method. Several specimens of SrAl₂O₄:Eu²⁺ phosphors with different Eu²⁺ concentrations, typically 0.1, 0.5, or 1 mol % were prepared by combustion synthesis. Combustion synthesis can produce more homogeneous products compared with the products prepared by the SSR method due to a proper mixing of the starting materials and a relatively low reaction temperature. The following starting materials were used: aluminum nitrate (Al(NO₃)₃ · 9H₂O; System, 98%), strontium nitrate (Sr(NO₃)₂; Aldrich, 99%), europium oxide (Eu₂O₃;

Aldrich, 99.99%) and urea ($\text{CO}(\text{NH}_2)_2$; System, 99%). A small amount of boric acid (H_3BO_3 ; Fisher, 100.04%) was used as a flux; small amounts of urea were used as both a reducer and a fuel. Each raw material— $\text{Al}(\text{NO}_3)_3 \cdot 9\text{H}_2\text{O}$, $\text{Sr}(\text{NO}_3)_2$, H_3BO_3 and $\text{CO}(\text{NH}_2)_2$ —was dissolved in deionized water; Eu_2O_3 was dissolved with a minimum amount of an HNO_3 solution to be converted to $\text{Eu}(\text{NO}_3)_3$. These two solutions were mixed together and stirred using a magnetic bar at 75°C for a few hours to obtain a viscous gel solution. A white combustion ash was obtained within 3–5 min by combusting the precursor gel at 500°C . The final synthesis of pigments was conducted by heating the combustion ash at 1000°C in a weak reductive atmosphere for 2 h to obtain a $\text{SrAl}_2\text{O}_4:\text{Eu}^{2+}$ phosphor. The weak reductive atmosphere was created by using a graphite crucible to inhibit further oxidation. The particle-size analysis results showed that the phosphor powder has an average size of 50 and 132 nm before and after calcinations, respectively. The grain sizes considerably exceed the effective radii of the impurity sites; for this reason, the excitation and emission spectra of the bulk crystals and the nanosized $\text{SrAl}_2\text{O}_4:\text{Eu}$ powder prove to be identical. In addition to the $\text{SrAl}_2\text{O}_4:\text{Eu}$ specimen (designated as CSAE, see Table 1), a codoped specimen of $\text{SrAl}_2\text{O}_4:\text{Eu,Dy}$ with optimized dopant concentrations (0.5 mol % Eu^{2+} and 5 mol % Dy^{3+} , designated as CSAED) and an undoped $\text{SrAl}_2\text{O}_4:\text{Eu}$ specimen (designated as CSA) were also prepared and studied.

2.2 Characterization techniques

X-ray diffraction (XRD) analysis. Phase identification was carried out using Bruker, D8 Advance X-ray Diffraction with $\text{Cu-K}\alpha$ radiation of wavelength 1.54 \AA was applied. Data have been collected by step-scanning 2θ from 10° to 90° and 0.034 s counting time at each step at room temperature.

Photoluminescence spectroscopy. The measurements of photoluminescence, luminescence excitation (PLE) spectra were performed using a laboratory setup. A 150 W Xe lamp combined with monochromator MDR-206 is used as an excitation source. The luminescence is detected using Oriel MS257 spectrograph equipped with Marconi 30-11 CCD detector. The samples are placed into vacuum optical cryostat Cryotrade LN-120, which allows to perform measurements in the temperature range 80 – 500 K.

The excitation spectra (Fig. 13) of the Eu^{2+} ion in the $\text{SrAl}_2\text{O}_4:\text{Eu}^{2+}$ materials were measured in an energy range of 3.7–20 eV using the synchrotron radiation at a SUPERLUMI station (Beamline I) of HASYLAB at DESY (Hamburg, Germany).

Scanning electron microscopy. The morphology and topography of the samples were observed by using scanning electron microscope (SEM) model Zeiss Supra 35 VP. The samples were placed on the pin mount specimen holders with the help of double-sided tape. The samples are coated with a few nanometers thick of gold palladium layer by using Sputter Coater Polaron SC 515 before SEM observation.

A special additional attachment with SEM to study the luminescent properties and CCL imaging was also used [15–18].

The experimental setup consists of a SEM "STEREOSCAN MK IIA" and a color cathodoluminescence attachment GA-Group CCL3i installed on it (Fig. 1).

A focused electron beam excites a small volume of a specimen mounted in the SEM sample chamber. The CL-radiation excited in the specimen by an electron beam is collected by a system of mirrors focused on the input window of the fiber-optic system and divided into three equivalent optical channels. Such collector allows us to collect more than 90% of the light flux, the solid angle of radiation collection $\approx 2\pi$.

For the CL-radiation spectral analysis in real colors, wideband overlapping light filters are used, having a transmission maximum at wavelengths of 450 nm (blue), 540 nm (green), and 670 nm (red), which are similar to color television spectral characteristics. After optical filtering, the CL signals are converted to electrical signals using photomultiplier tubes, digitized, and stored in the memory of the CCL-SEM attachment. The digital scan generator drives the SEM deflection system and forms the user-defined raster on the specimen surface. The generated digital SEM image is transferred over a local network to display and personal computer for mathematical processing. The use of light filters for spectral analysis and highly sensitive photomultiplier tubes provides the maximum possible sensitivity, which makes it possible to study radiation-unstable materials at low beam currents and low radiation doses. The use of electron beam blanking and low sweep speeds provide sharp images of materials with a long afterglow time.

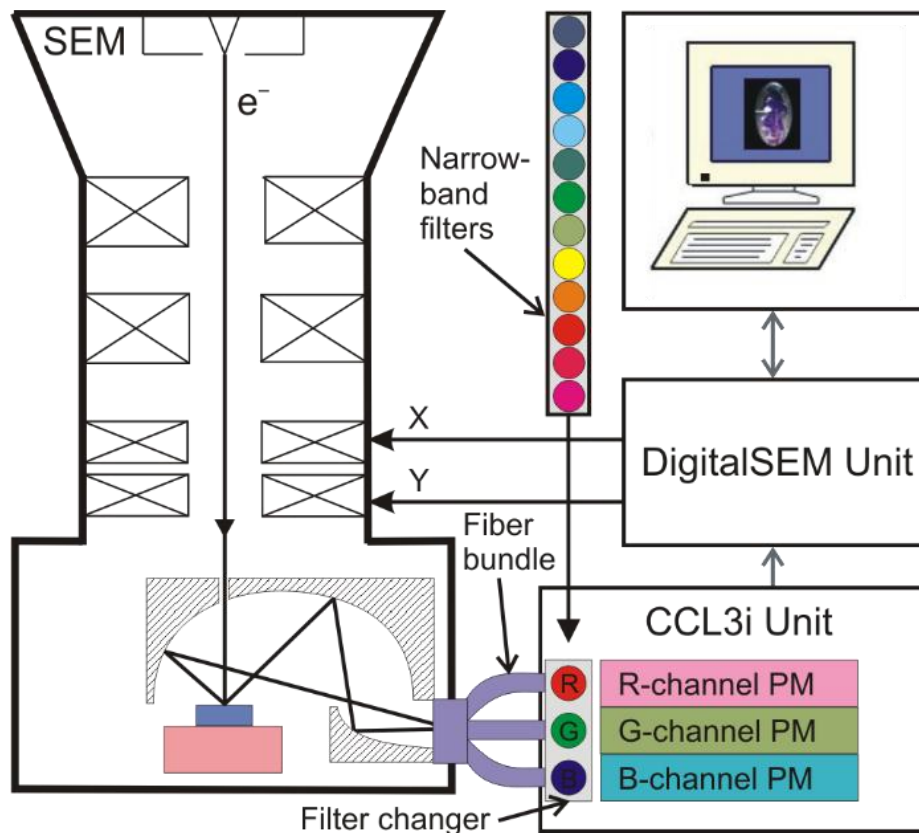


Fig. 1. Color cathodoluminescence imaging setup.

The acquisition and storage of additional SEM-signals, such as secondary electrons (SE), backscattered electrons (BSE), and induced current (IC) gives additional possibilities for specimen analysis. Combination of different SEM-modes data into one color composite image makes it possible to reveal the spatial correlation between the specimen topography, the location of electrical potential barriers and CL-center distribution.

3. Results and Discussion

3.1. Structure, morphology and luminescence

Exciting by UV or sun light this phosphor shows bright blue-green luminescence (Fig.2).



Fig. 2. Bright luminescence of $\text{SrAl}_2\text{O}_4:\text{Eu}^{2+},\text{Dy}^{3+}$ based phosphor in the open air under sun light excitation.

After some time, when the excitation is turned off, emission from previously trapped electrons is still observed in persistent phosphor $\text{SrAl}_2\text{O}_4:\text{Eu}^{2+}$ (Fig. 3).

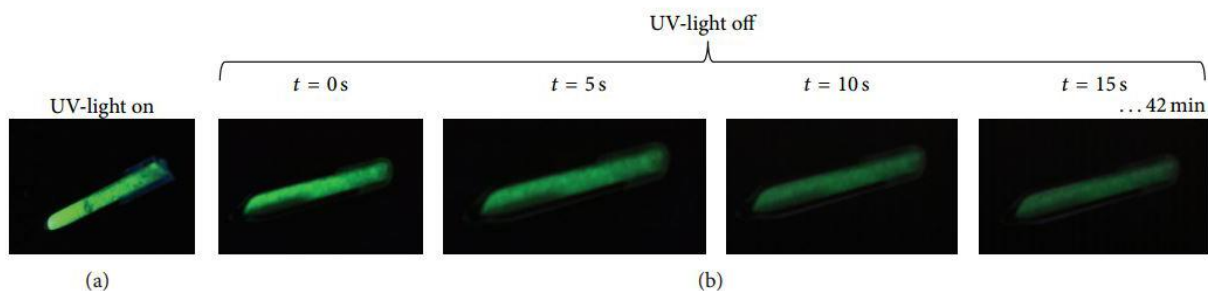


Fig. 3. Green luminescence of $\text{SrAl}_2\text{O}_4:\text{Eu}^{2+}$ under UV light (left, a) and afterglow effect with duration of up to 42 min after turning the UV light off (right, b).

The mechanism of long persistent phosphors' phosphorescence is basically a three-level electron transition mechanism, which includes a ground state, an excited state, and a meta-stable trapping state. The phosphorescence lifetime is usually longer than the lifetime at the excited state, and it depends on the trap depth and trapping/detrapping mechanism.

X-ray diffraction patterns of strontium aluminate codoped with Eu^{2+} and Dy^{3+} (SAED) obtained at 1250°C with different Eu^{2+} concentrations are shown in Fig. 4. The major formed phase is monoclinic SrAl_2O_4 and corresponds to the standard JCPDS card data (74-0794). The secondary observed phase corresponds to $\text{Sr}_4\text{Al}_{14}\text{O}_{25}$. This result indicates that the reaction conditions in this study are sufficient to obtain multiphase $\{\text{SrAl}_2\text{O}_4+\text{Sr}_4\text{Al}_{14}\text{O}_{25}\}:\text{Eu}^{2+}$ phosphors. Small changes in the activator concentration do not have any effect on the phase formation.

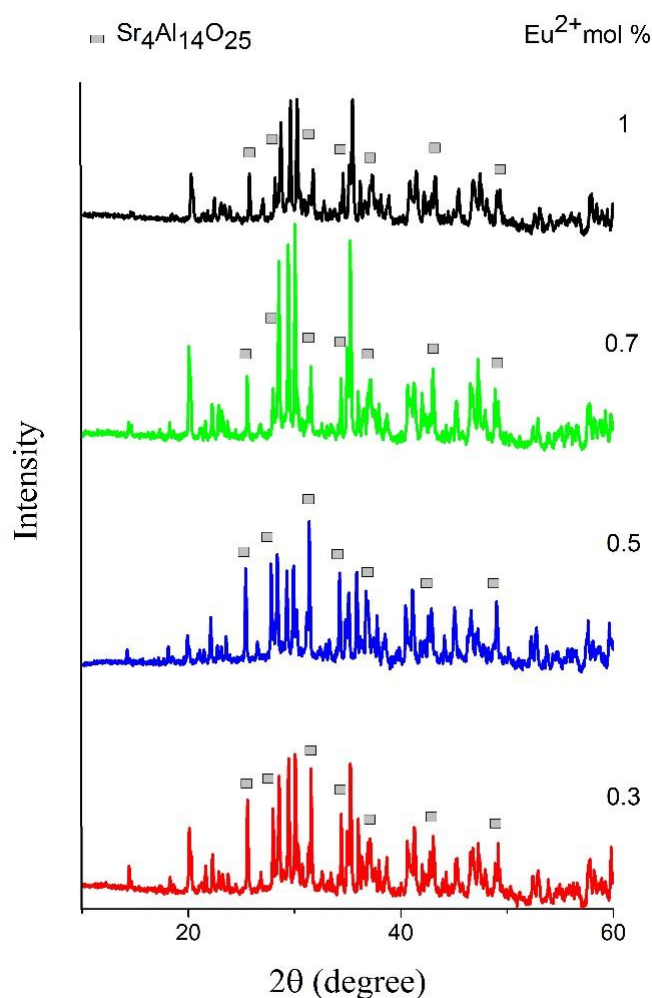


Fig. 4. X-ray diffraction patterns of phosphors at different Eu^{2+} concentrations.
[\square = $\text{Sr}_4\text{Al}_{14}\text{O}_{25}$, JCPDS 52-1876, unmarked peaks correspond to SrAl_2O_4 , JCPDS 74-0794]

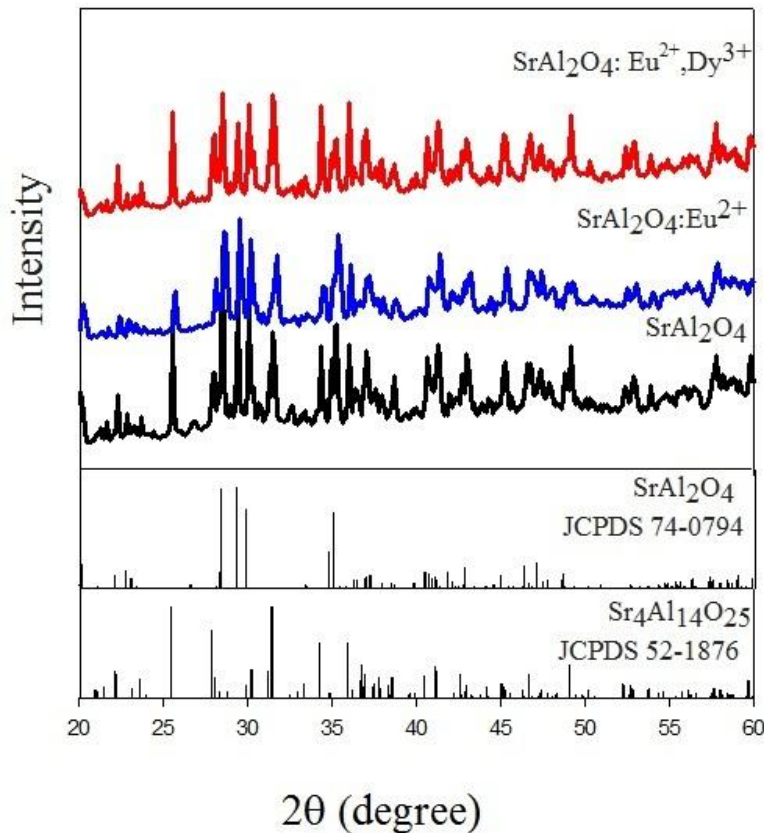


Fig. 5. X-ray diffraction patterns of the synthesized SA, SAE and SAED phosphors.

Figure 5 shows the main XRD patterns of SA, SAE, and SAED specimens annealed at 1250°C for 2 h in an active carbon atmosphere. It is evident from Figs. 4 and 5 that the XRD patterns include two phases, namely, SrAl_2O_4 and $\text{Sr}_4\text{Al}_{14}\text{O}_{25}$; this fact indicates the formation of mixed oxide phases. After annealing, the XRD peaks become sharper and stable phases of SrAl_2O_4 and $\text{Sr}_4\text{Al}_{14}\text{O}_{25}$ with higher crystallinity are formed.

3.2. Scanning electron microscopy analysis

Microscopy and topography analysis of the phosphorescent powders was conducted by SEM. The main idea is to observe any crystallized phases present in the specimens.

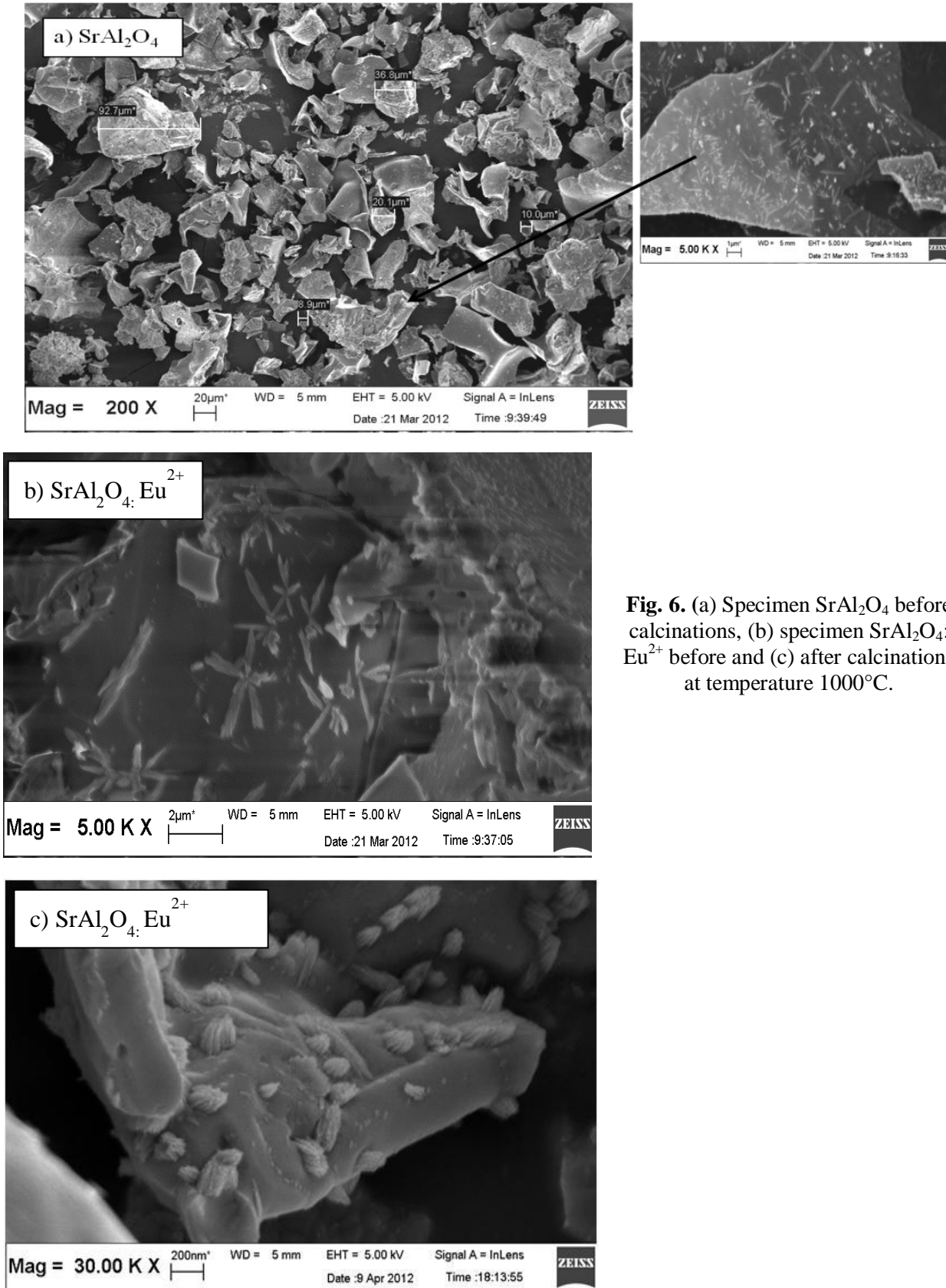


Fig. 6. (a) Specimen SrAl₂O₄ before calcinations, (b) specimen SrAl₂O₄:Eu²⁺ before and (c) after calcinations at temperature 1000°C.

Figure 6a shows the morphology of the SrAl_2O_4 host material without adding any activator and coactivator, while Figs. 6b and 6c show the $\text{SrAl}_2\text{O}_4:\text{Eu}^{2+}$ specimens with an additional europium activator. Figure 6a shows the particle size distribution obtained from SEM for specimen SrAl_2O_4 before calcinations. It is clearly seen from the figure that an irregular structure at various sizes and lengths were obtained. All the specimens show the formation of crystal structures of the phosphor. The homogenous distribution and size of the star-like structure on the matrix surface shows that the activator ions were homogenously dispersed throughout the phosphor matrix. In the case of an additional amount of Eu, specimen $\text{SrAl}_2\text{O}_4:\text{Eu}^{2+}$ (Fig. 6b) has higher crystallite or star-like particles compared with those of specimen SrAl_2O_4 . The particles connected together form a larger network of a star-like structure. The crystal structure has a clear, longer and same size in each leg of the star-like particles. After calcinations at 1000°C and a soaking time of 2 h, the particles with a star-like structure of specimen $\text{SrAl}_2\text{O}_4:\text{Eu}^{2+}$ closed and stacked together to form a flower-like structure with higher crystallinity (Fig. 6c).

The possible mechanism of formation of a flower-like structure can be described as shown in Fig. 7. Generally, the crystal growth process involves two stages: nucleation and growth. The particles undergo nucleation at the initial state. With an increase in temperature, the grains become compressed and more fined. The needle shape and star-like structure appear after 500°C . This structure is unstable and agglomerate during calcinations at 1000°C to form a stable specific flower-like structure.

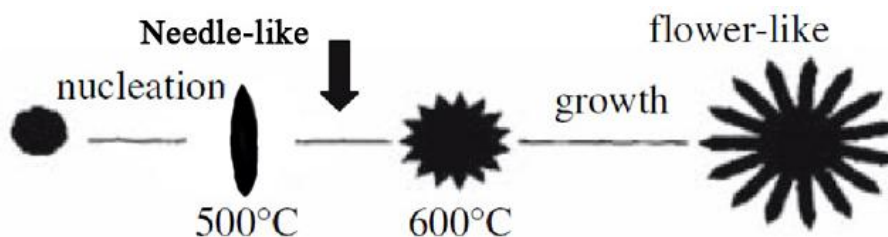


Fig. 7. Schematic illustration of the possible mechanism of formation of a flower-like structure of $\text{SrAl}_2\text{O}_4:\text{Eu}^{2+}$.

3.3. Photoluminescence spectroscopy

The emission spectra of the CSAE-1 and SAE-1 phosphors are shown in Figs. 8 and 9. The spectrum of the CSAE specimen is characterized by a broad emission band peaking at 520 nm at room temperature. The narrow line at 615 nm corresponds to emission from Eu^{3+} ions, while the weak hump at 400 nm is attributed to defect-related emission centers [14]. The band at 520 nm can be approximated by a single Gauss curve. The obtained result shows that CSAE specimens are characterized by a single SrAl_2O_4 phase.

The emission spectra of specimens from the SAE and SAED sets are shifted to low-wavelength region relatively to that of the CSAE specimen. (SAED spectra are not shown here; however, they are very similar to those of the SAE specimen). The bands are asymmetric and decomposed using two Gauss curves with maxima at 520 nm and 490 nm. These bands correspond to Eu^{2+} emission in the $\text{Sr}_4\text{Al}_{14}\text{O}_{25}$ (490 nm) and SrAl_2O_4 (520 nm) phases. Therefore, PL spectroscopy confirms the presence of two phases in SAE and SAED series.

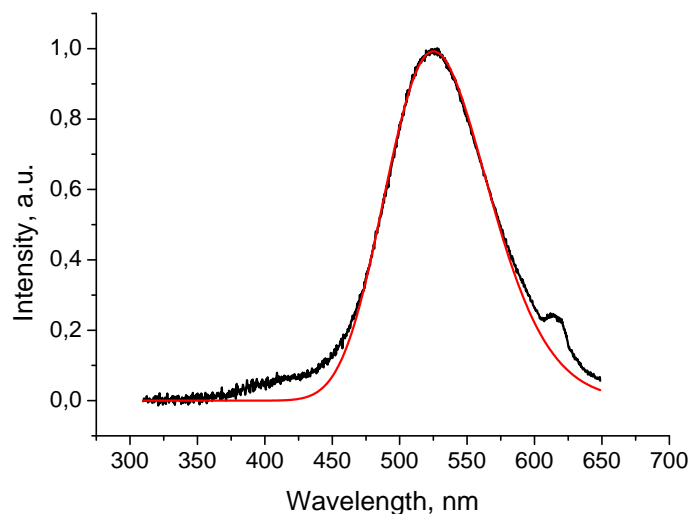


Fig. 8. Photoluminescence spectrum of the CSAE-1 phosphor (black line) and the spectrum approximation by a single Gauss curve (red line), $T = 300$ K, $\lambda_{\text{ex}} = 300$ nm. Gauss fit was performed in eV scale and then spectra were replotted in nm scale. Conversion between eV and nm scales was performed with account of the λ^2 factor.

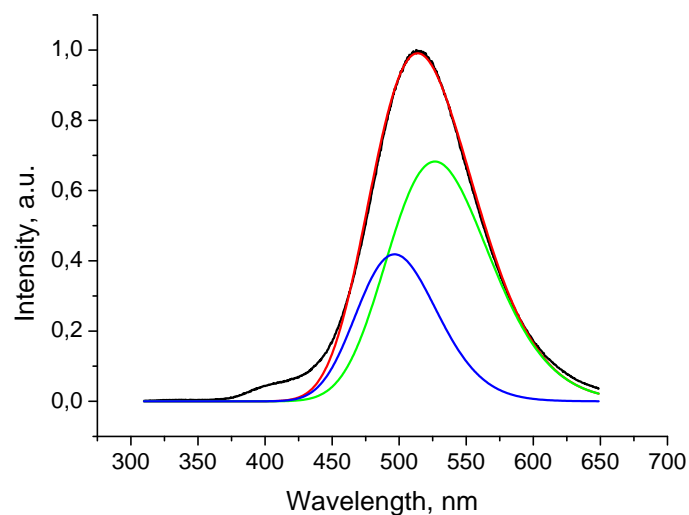


Fig. 9. Photoluminescence spectrum of the SAE-1 phosphor and the spectrum decomposition on two Gauss components, $T = 300$ K, $\lambda_{\text{ex}} = 300$ nm. Gauss fit was performed in eV scale and then spectra were replotted in nm scale. Conversion between eV and nm scales was performed with account of the λ^2 factor.

Photoluminescence properties were studied in a temperature range of 100–500 K to determine whether the synthesized phosphors are suitable for use in fabrication of pc-white LEDs (pc-WLEDs). For instance, measurements of luminescence spectra at high temperatures (up to 400 K) are required to verify whether the synthesized nanophosphors are stable at high temperatures for the application in LEDs operating at temperatures exceeding the room temperature.

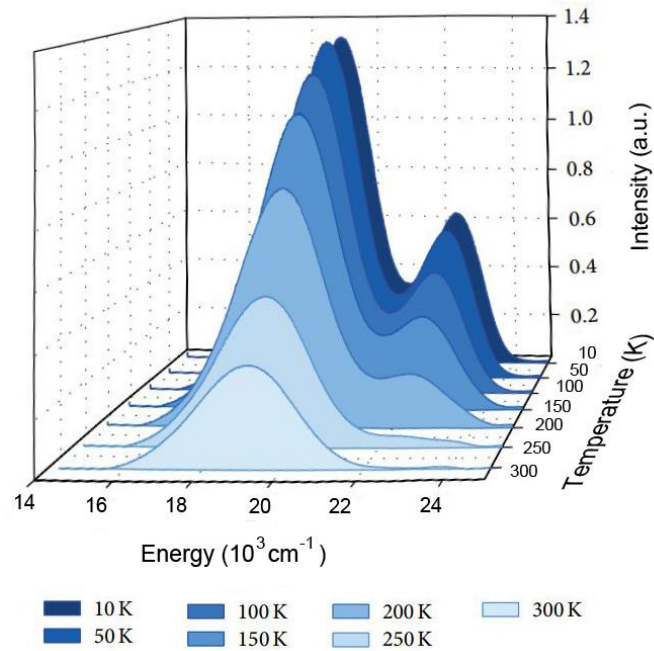


Fig. 10. Effect of decreased temperatures on the emission spectrum ($\tilde{\nu}_{\text{ex}} = 27620 \text{ cm}^{-1}$).

During the heating of the specimen from 10 K to room temperature (Fig. 10) and up to 500 K (Fig. 11), a gradual decrease of the overall emission intensity is observed. This behavior is expected due to the loss of energy owing to nonradiative transitions at higher temperatures.

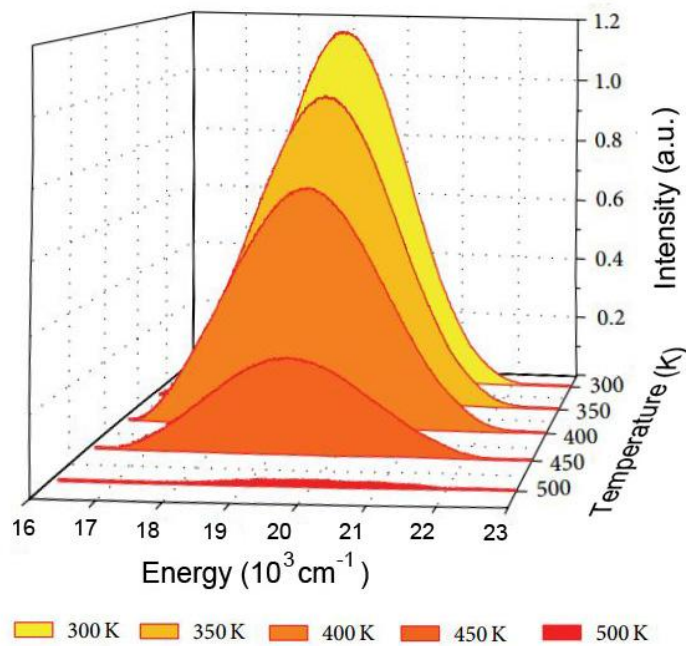


Fig. 11. Effect of increased temperatures on the emission spectrum ($\tilde{\nu}_{\text{ex}} = 27620 \text{ cm}^{-1}$).

The common feature of various solid state materials, which are doped with Eu^{2+} , is an intense broad band luminescence originating from the transitions between the $^8\text{S}_{1/2} (4f^7)$ Eu^{2+} ground state and the crystal field components of the $4f^6 5d^1$ excited state [19]. Our experiments show that the emission spectrum consists of one band peaking at around 520 nm at room temperature and two broad PL bands at 450 and 520 nm wavelengths at low temperatures (2.75 eV and 2.42 eV, respectively). At room temperature, only the low energy band is observed, since the 450 nm band is nearly quenched. These experimental results are shown in Fig. 12.

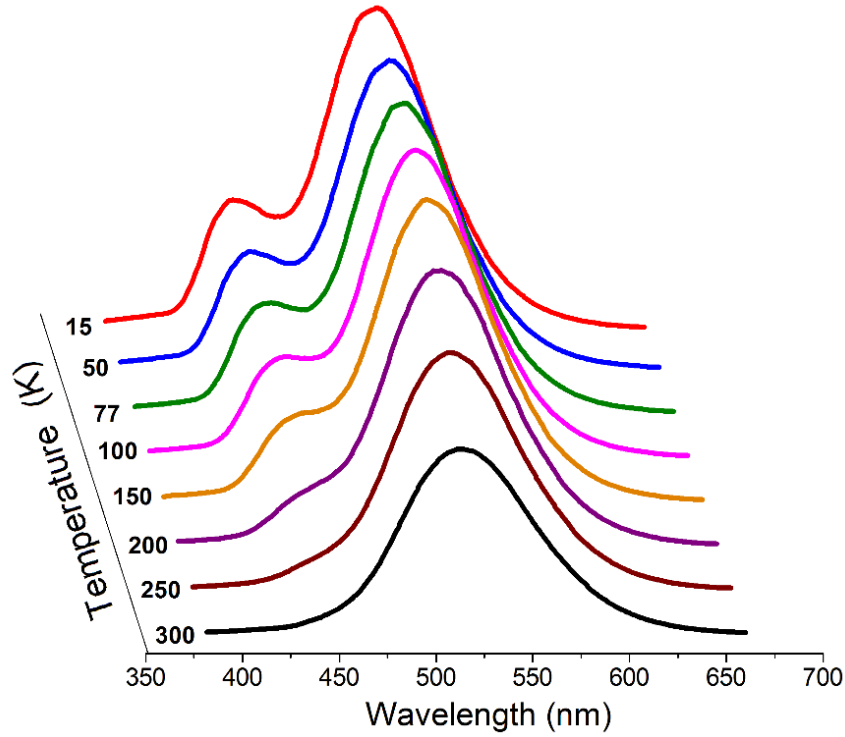


Fig. 12. Emission spectra ($\lambda_{\text{ex}} = 325$ nm) of $\text{SrAl}_2\text{O}_4:\text{Eu}^{2+}$ at different temperatures.

The luminescence at 520 nm is commonly ascribed to the parity-allowed electric dipole transition ($4f^6 5d^1 \rightarrow 4f^7$) of the Eu^{2+} ion [20]. The origin of the 450-nm emission is still under discussion. Poort et al. [21] suggested that the 450 and 520 nm emission bands originate from the emission of the Eu^{2+} ion located at two different crystallographic strontium sites. Clabau et al. criticized such assignment and proposed that the 450 nm band arises from the charge transfer from oxygen to the residual Eu^{3+} ion that takes place upon UV irradiation and is associated with a hole trapping at Sr^{2+} vacancies [22].

The appearance of two bands can be explained by the fact whether preferential orientation of the d -orbitals occurs (Sr_2 site) or not (Sr_1 site) [21]. Eu^{2+} ions entering the Sr_1 sites show broad emission at a higher energy (at 450 nm), and those ions at the Sr_2 sites cause the lower energy band. Both Sr sites occur almost in equal amounts in the host lattice.

The total integrated luminescence intensity of both bands hardly changes in a temperature range of 15–150 K and decreases significantly when the temperature is raised above 150 K. This

effect is caused by temperature luminescence quenching. With an increase in temperature above 250 K, the blue band at 450 nm completely disappears due to energy transfer. A separate study of the behavior of the bands at low temperatures shows that the integrated intensity of one of the luminescence bands (450 nm) decreases, while the intensity of the other band (520 nm) increases. That is why it is reasonable to assume the existence of a nonradiative energy transfer between these two bands. In $\text{SrAl}_2\text{O}_4:\text{Eu}^{2+}$, the energy transfer is very effective, because the critical transfer distance R_c between inequivalent Eu^{2+} ions is large ($\sim 14 \text{ \AA}$) [21].

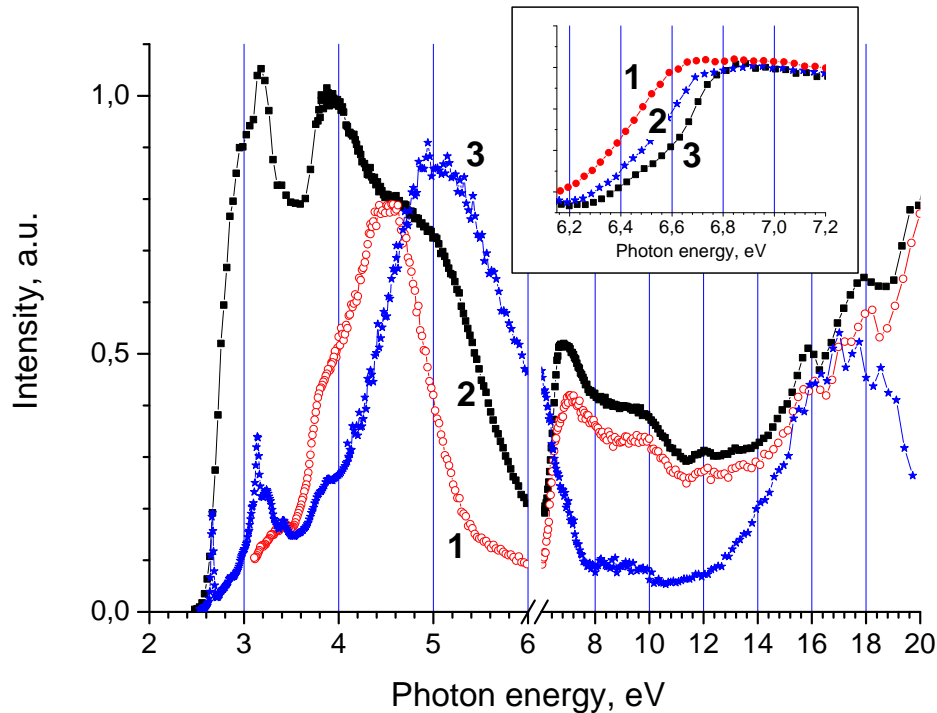


Fig. 13. Luminescence excitation spectra of $\text{SrAl}_2\text{O}_4:\text{Eu}^{2+}$ measured for $\lambda_{\text{em}} = (1)$ 400, (2) 510, and (3) 620 nm at $T = 300 \text{ K}$. In the inset: excitation spectra measured in the region of fundamental absorption edge for $T = (1)$ 300, (2) 150, and (3) 10 K for $\lambda_{\text{em}} = 510 \text{ nm}$.

The excitation spectra of the emission bands observed in $\text{SrAl}_2\text{O}_4:\text{Eu}^{2+}$ are shown in Fig. 13. The structure of the excitation spectra for the bands peaking at 450 nm (2.75 eV, curve 1) and 520 nm (2.42 eV, curve 2) is substantially different in an energy region of 2.5–6.0 eV, which corresponds to the direct excitation of the emission centers. It indicates that different positions of the energy levels of the centers are responsible for these two emission bands. Above 6.0 eV, an abrupt rise is observed for both excitation spectra. The excitation in this energy region can be attributed to the energy transfer from the host states of the matrix to the emission centers; in addition, transitions from the valence band to the conduction band also contribute to the formation of these spectral features. This conclusion has been presented earlier on the basis of analysis of the excitation spectra of 520 nm emission in $\text{SrAl}_2\text{O}_4:\text{Eu}^{2+}$ in [23] and the excitation

spectra of the host emission in $\text{SrAl}_2\text{O}_4:\text{Eu}^{2+},\text{Dy}^{3+}$ in [27]. With a further increase in the excitation energy, the features of the structure are also common for the spectra. Similar behaviors of the excitation spectra for both emission bands in the region above the band gap E_g implies similar mechanisms of the energy transfer from the host to these emission centers. The increase in the intensity at $E > 14$ eV is associated with the multiplication of the electronic excitations when the energy of the one excitation photon is sufficient for the formation of two electron–hole pairs.

The energy of the lowest interband transitions can be deduced from the analysis of the excitation spectra of the emission band with maximum at 520 nm. Previously, the band gap was determined to be about 6.5 eV by Palilla et al. [20] or 6.6 eV by Holsa et al. [23]. To our opinion the value is slightly underestimated, because it does not account for the possible formation of excitons in SrAl_2O_4 . The threshold of the excitation spectra is shifted to the high-energy region with the cooling of the specimen (see inset in Fig. 13). This behavior is characteristic of the excitation at the edge of the fundamental absorption region in the insulators. The shift frequently obeys the Urbach rule, which implies the formation of excitons with the energy exceeding the region of the abrupt increase in the intensity in the region of the threshold. Taking this consideration into account, the band gap can be estimated as $E > 6.5$ eV for SrAl_2O_4 .

Some of the studied specimens of $\text{SrAl}_2\text{O}_4:\text{Eu}^{2+}$ also exhibited red emission related to unreduced Eu^{3+} ions (Fig. 8). The excitation spectrum of this emission is also shown in Fig. 13 (curve 3). The excitation spectra of the Eu^{3+} related emission band exhibit sharp peaks at 2.65 and 3.12 eV, which are attributed to the excitation via $4f-4f$ transitions (${}^7\text{F}_0$ to ${}^5\text{D}_2$ and ${}^5\text{L}_6$ levels, respectively). The intensive excitation band with maximum at 5 eV is a charge transfer band that arises due to the electron transitions from the oxygen $2p$ states to the $4f$ orbitals of europium, which agrees with previous experimental results and our theoretical calculations [24].

3.4. Study of phosphors using the CCL–SEM method

The specimens were mounted on a holder using a graphite conductive tape. Poorly adhered powder particles were removed using compressed air. Thin (<0.5 μm) gold layer was deposited on the surface of the specimens to eliminate the charging effect. All specimens from synthesis #1 and #2 and from different sets were studied in CCL and SE modes at various magnifications and scanning parameters.

The CCL images show that SAED and SAE specimens have inhomogeneous CL, both in intensity and in spectrum (Fig. 14). There is no fundamental difference in CCL between series from synthesis #1 and #2. The green luminescence areas correspond to the emission of Eu^{2+} in the SrAl_2O_4 phase (emission is peaking at 525 nm according to Fig. 9), areas with blue luminescence areas are due to Eu^{2+} in the $\text{Sr}_4\text{Al}_{14}\text{O}_{25}:\text{Eu}^{2+}$ phase (emission is peaking at 490 nm). Thus, these specimens can be considered as a mixture of two phases or multiphase blue-green $\{\text{SrAl}_2\text{O}_4+\text{Sr}_4\text{Al}_{14}\text{O}_{25}\}:\text{Eu}^{2+},\text{Dy}^{3+}$ phosphors. If the luminescence is excited by a wide beam, as in case of PL, the integral spectrum from two phases $\{\text{SrAl}_2\text{O}_4+\text{Sr}_4\text{Al}_{14}\text{O}_{25}\}:\text{Eu}^{2+},\text{Dy}^{3+}$ will be observed and the spectrum maximum will be between 520 and 490 nm. The spectrum maximum position will depend on the volume ratio of the phases; by changing this ratio, it is possible to tune the emission color in a range of 490–520 nm.

In addition to the CCL mode, all specimens were studied in the BSE or SE mode and also in combined CCL and SE modes at various magnifications and scanning parameters. The results of the study in the different modes are shown in Fig. 15.

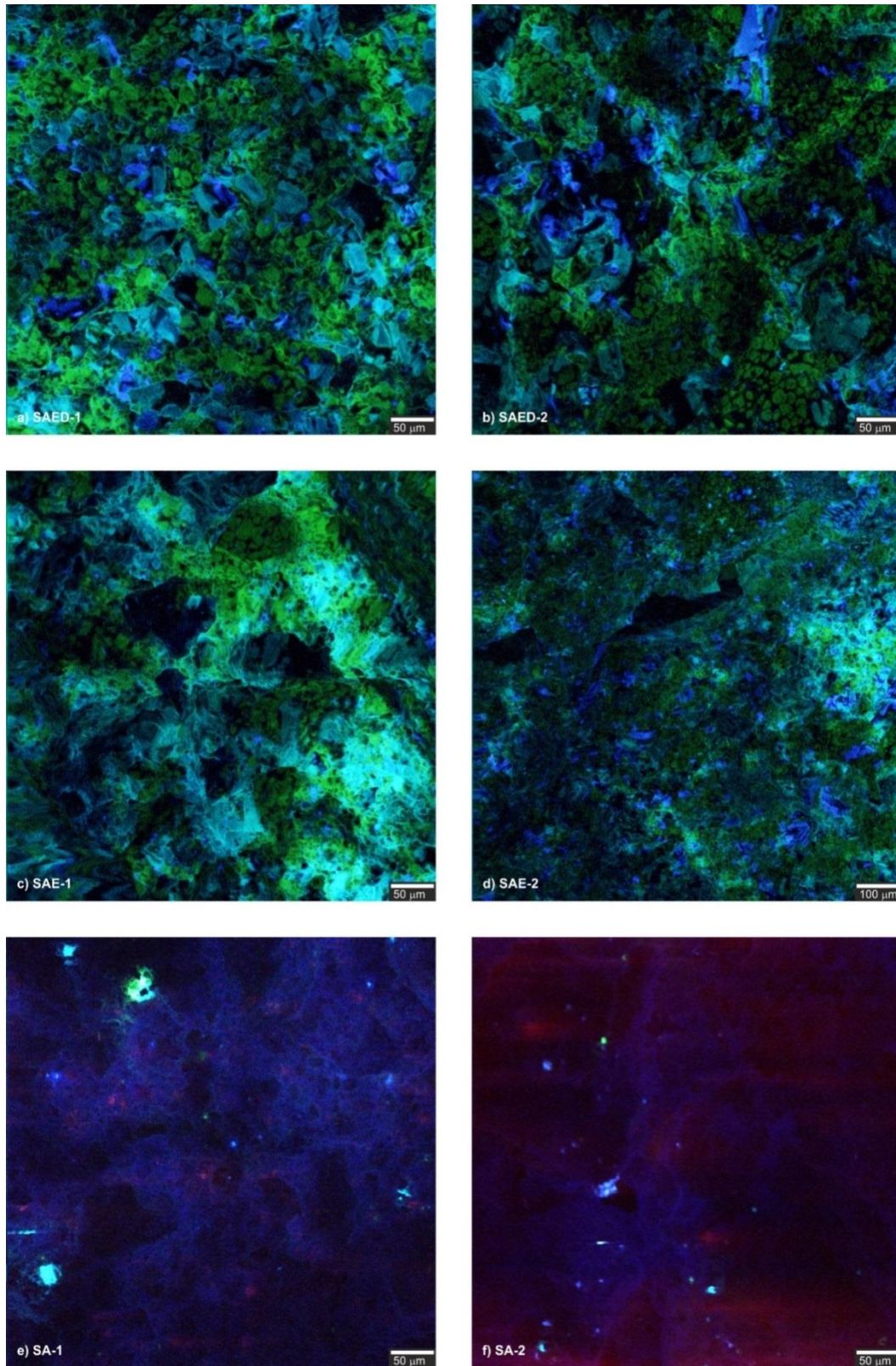


Fig. 14. Color cathodoluminescence images of the specimens prepared by SSR at low magnifications. Horizontal field width is 500 μm.

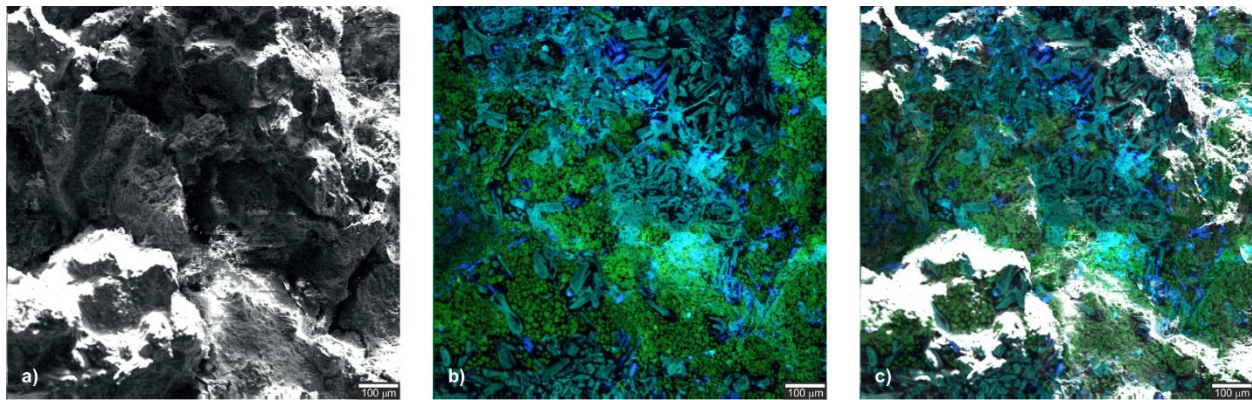


Fig. 15. CCL–SEM images of SAED-1 in the different modes: (a) SE, (b) CCL, and (c) SE+CCL. Horizontal field width is 1000 µm.

Composite CCL+SE contrast in scanning microscopy is a new type of SEM mode, which is a fairly promising tool for studying luminescence materials. The (CCL+SE)–SEM images with both a fine structure and color information can simplify the observation, interpretation, and analysis of different nature specimens, because the human eye is essentially an organ for observing color and can distinguish thousands of color hues and intensities.

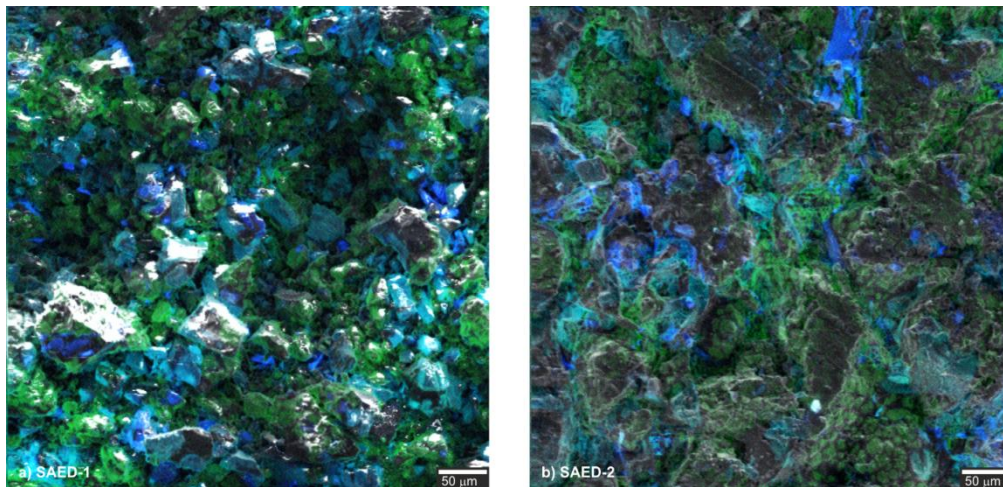


Fig. 16. Two powders from the SAED series prepared under similar conditions in the CCL+SE composite contrast mode. Horizontal field width is 500 µm.

Figure 16 shows images of the SAED-1 and SAED-2 specimens recorded using the CCL+SE composite contrast mode of operation. These images can be interpreted as CCL images (similar to Figs. 14a, 14b) superimposed on the relief of the specimen obtained using secondary electrons. In this way, accurate data on the correlation between luminescent properties and surface relief are provided.

These images show that regions with a low CL intensity are located mostly on large particle faces. Since the CL emission depends on the dopant concentration, it can be assumed that the CL heterogeneity is a consequence of an uneven distribution of the dopant during

microcrystal growth. However, this effect can be also associated with a large number of nonradiative recombination channels due to increased defect formation in some particles.

The SAE-1 and SAE-2 specimens have similar heterogeneous CL, both in intensity and in spectrum. There are no pure blue regions on the SAE-1 specimen corresponding to the $\text{Sr}_4\text{Al}_{14}\text{O}_{25}:\text{Eu}^{2+}$ phase. Therefore, in this specimen, the phases are mixed much stronger than in SAE-2 specimen. The SA-1 and SA-2 specimens (Figs. 14e, 14f) have a much weaker luminescence emission. The spectrum contains weak blue and red parts associated with the luminescence of the intrinsic SrAl_2O_4 defects or artefacts. Less expressed CL inhomogeneity is caused by the absence of doping ions.

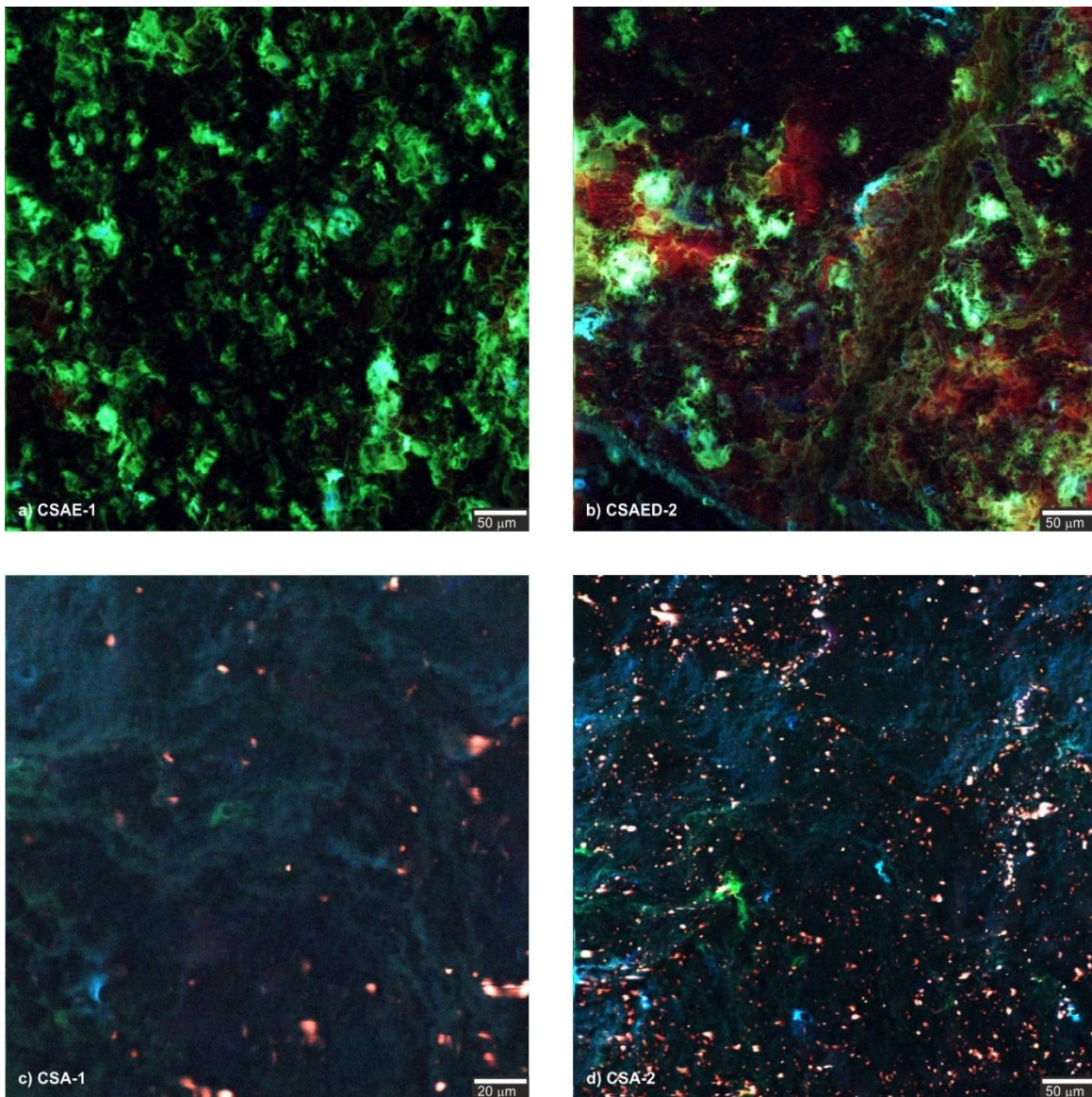


Fig. 17. Color cathodoluminescence images of the specimens prepared by the combustion method at low magnifications. Horizontal field width is 500 μm .

Specimens CSAE-1 and CSAED-2 (Figs. 17a, 17b) produced by combustion synthesis, differ from the specimens synthesized by SSR (Fig. 14) and mostly consist of single SrAl_2O_4 phase. However, there are some red luminescence areas, which can be associated with the presence of Eu^{3+} ions in the SrAl_2O_4 phase. It is also confirmed by a small red peak at 615 nm in the PL emission spectra (Fig. 8).

The more detailed quantitative interpretation of the PL and PLE spectra and the thermoluminescence of these specimens will be given in a forthcoming paper.

4. Applications

Applications of persistent luminescence phosphors are rapidly expanding from bulk materials visible to everyone (e.g., exit signalization on airplane cabin floors) to high-tech products. Persistent phosphors are used in signalization, traffic signs, power switch, traffic police uniforms, luminous paints, glow-in-the-dark toys, decorative objects, emergency signage, watches and clocks, dials and displays, textile printing, medical diagnostics, and many other applications. In this review, we discuss conventional applications, such as LED, biology, painting, and decoration. In addition, we propose a new direction in the research and application of these materials, namely, underwater studies of persistent luminescence for an artificial reef and algae cultivation.

4.1. Light-emitting diodes

Nanophosphors play an important role in the manufacture of pc-LEDs. Unlike microphosphors, nanoparticles reduce internal scattering inside the material. This property is very useful for eliminating losses due to the scattering of the emitted light back into the primary semiconductor light crystal, which prevents chip heating.

SrAl₂O₄:Eu²⁺-based LED coat. In pc-WLEDs, noble phosphor materials play a crucial role in high quality white emission. Luminescent nanosized particles exhibit some advantages over analogous bulk specimens, such as high packing density, low light scattering effects, and energy saving synthesis (with a shorter preparation time and lower sintering temperatures); they are readily suspendable in liquid media. Due to the small size, nanosized particles are able to build thinner films, for example, on the surface of LEDs, and are less subjected to concentration quenching effects compared with doped micron-sized phosphors. For LED applications, the prepared nanosized particles were combined with an InGaAlN-based UV LED chip (chip size of $400 \pm 25 \mu\text{m} \times 400 \pm 25 \mu\text{m}$, thickness of $80 \pm 10 \mu\text{m}$) as an optical pumping source, and the performance of the prepared LEDs was studied. Phosphor-converted LEDs were fabricated by combining UV LED as an optical pumping source with post-heat-treated $\text{SrAl}_2\text{O}_4:\text{Eu}^{2+}$ nanosized particles. The nanosized particles were mixed with a transparent silicone gel (1 : 10 wt %) and coated onto a lead frame with an UV chip with maximum emission at about 350 nm. Figure 18 shows the emission spectrum (Lab Sphere) of the fabricated LEDs.

The $\text{SrAl}_2\text{O}_4:\text{Eu}^{2+}$ nanosized particles were excited with UV light and generated green emission. The CIE-1931 coordinates of $\text{SrAl}_2\text{O}_4:\text{Eu}^{2+}$ phosphors conversion LEDs were in the green region at 20 mA ($x = 0.288$, $y = 0.547$, Fig. 18). The excitation intensity and respective emission peak showed that $\text{SrAl}_2\text{O}_4:\text{Eu}^{2+}$ was a suitable green phosphor for UV excited WLEDs.

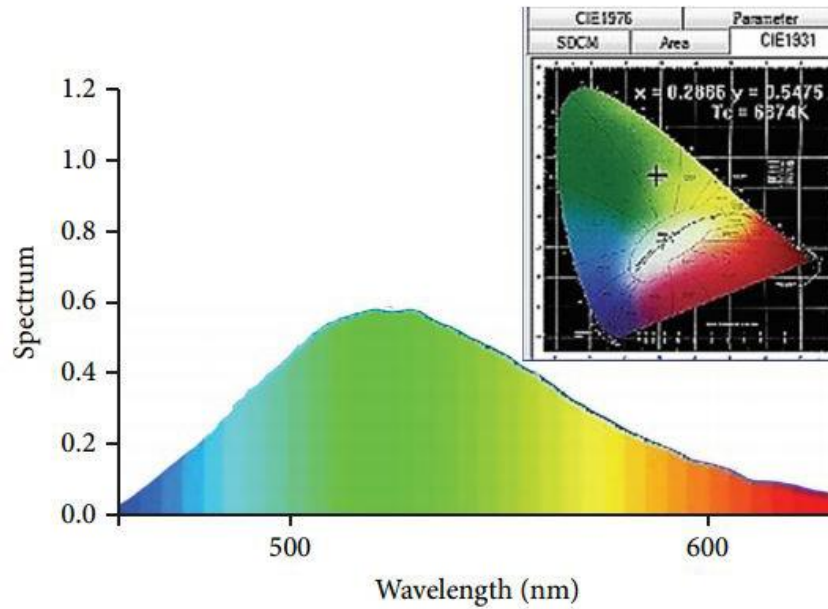


Fig. 18. Emission spectrum and CIE-1931 coordinates of the prepared LED.

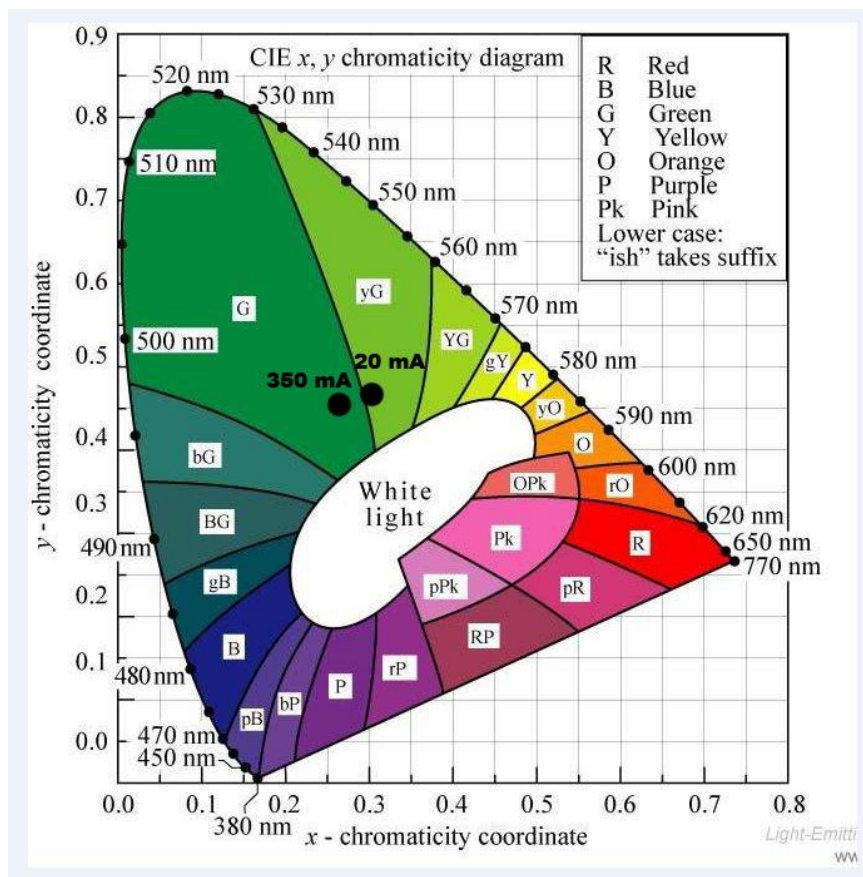


Fig. 19. Color coordinates of pc-LEDs based on SrAl₂O₄:Eu (1%) under $I_f = 20, 350$ mA in the CIE chromaticity diagram.

Figure 19 shows the light parameters of another prepared pc-LED measured at two different currents (20 mA, 350 mA). For the preparation of a green pc-LED, the synthesized $\text{SrAl}_2\text{O}_4:\text{Eu}^{2+}$ (1%) nanophosphor and silica gel mixture was coated with a thin layer on an UV LED (365 nm) chip. The nanophosphor is very well excited by 365 nm and corresponds to the green region in a CIE chromaticity diagram with peaks of 550 nm at 20 mA and 535 nm at 350 mA (Fig. 19). Figure 19 shows the dependence of the color coordinate of the prepared green LED on different forward-bias currents ($I_f = 20, 350$ mA) plotted in a CIE 1931 chromaticity diagram. This diagram confirms that the prepared pc-LED is in the green region; the color coordinates are $x = 0.288$ and $y = 0.47$ at 20 mA. It is observed that the color coordinates of the prepared pc-LED are slightly shifted at different currents; this finding provides still more evidence that it is a stable ideal green-emitting phosphor for use in the preparation of WLEDs.

4.2. Persistent phosphors for painting and decoration



Fig. 20. Blue, red, pink, violet, yellow, and green colors are possible in glow dark paint.

Phosphorescent paint is commonly called “glow-in-the-dark” paint (Fig. 20). It is made of different phosphors, such as silver-activated zinc sulfide, or, more recently, doped strontium aluminate, and typically glows a pale green to greenish blue color. The mechanism for producing light is similar to that of fluorescent paint; however, the emission of visible light persists for some time after it was exposed to light. Phosphorescent paints have a sustained glow, which lasts up to 12 h after exposure to light; however, they eventually fade over time.

This type of paint has been used to mark escape paths in aircraft and for decorative use, such as “stars” applied to walls and ceilings (Fig. 21).



Fig. 21. Glow-in-the-dark rocket, planets, and stars wall stick.

Some other examples of glow-in-the-dark application are shown in Figs. 22–25.



Fig. 22. Hand-painted glow-in-the-dark blue Angelfish art magnet.



Fig. 23. Luminescent paint by Pieter van den Bosch.



*Floor
Tiles*

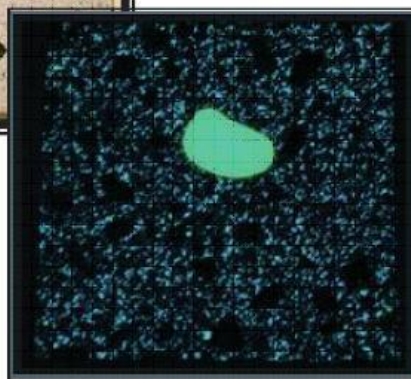


Fig. 24. Decorative floor tiles.



Fig. 25. A helmet and a high-voltage insulator (ceramic) in the day time and at dark.

4.3. Biological applications

There is a risk damaging the existence of thousands natural reefs forever because of tsunami or other cataclastic phenomena. We should know how to restore or, sometimes, improve reefs and marine ecosystems. Therefore, measuring and interpreting the impact of human actions on the diversity on marine and oceanic life represent one way to prevent ecological disasters and predict possible environmental changes.

We propose that an experimental artificial glow reef should be made of steel slag, concrete, and sand to provide a hard surface. Another decision is to cover this artificial reef and real corals with persistent phosphors. The main goal of these experiments is to cultivate the algae in future and attract fish. An artificial block made of concrete and sand and covered with a $\text{SrAl}_2\text{O}_4:\text{Eu}^{2+},\text{Dy}^{3+}$ based phosphor has been constructed; a new direction in the research and application of persistent phosphors has been proposed. For the first time, the underwater luminescence has been experimentally studied under real sea conditions. Our pioneering studies in this field have been published recently [25, 26].

Below, we show some applications of artificial reefs made of metallic construction and slag with persistent phosphors under real sea conditions near Malaysia in the Indian Ocean.

The real underwater experiments under sea conditions were carried out in Pulau Payar, Malaysia. First, artificial blocks covered with $\text{SrAl}_2\text{O}_4:\text{Eu}^{2+},\text{Dy}^{3+}$ and excited by the sun light were installed on the ocean floor with different relief (agropora corals, rocks, sand) and at varying depth of 2–6 m. Figure 26 shows the installation of an artificial luminescent block on a real stone in the sea at a depth of about 5 m.



Fig. 26. Installation of a concrete matrix covered with $\text{SrAl}_2\text{O}_4:\text{Eu}^{2+},\text{Dy}^{3+}$.

The next step was underwater luminescence studies. All the blocks showed a bright blue-green luminescence from all the places regardless of relief and depth. An example is shown in Fig. 27.



Fig. 27. Blue–green color luminescence of $\text{SrAl}_2\text{O}_4:\text{Eu}^{2+},\text{Dy}^{3+}$ at a depth of 5 m under real sea conditions.

After some minutes, fish was interested in a new luminescent object and gathered around it (Fig. 28).



Fig. 28. Fish is attracted by bright and long-lasting luminescence of $\text{SrAl}_2\text{O}_4:\text{Eu}^{2+},\text{Dy}^{3+}$.



Fig. 29. Clown fish is attracted by the bright light of the artificial reef.

Finally, the black-tip shark was also interested in luminescence and came near our artificial specimen (Fig. 30)



Fig. 30. Black-tip shark is also interested in luminescence.

Artificial coral reefs are shown in Figs. 31–34.

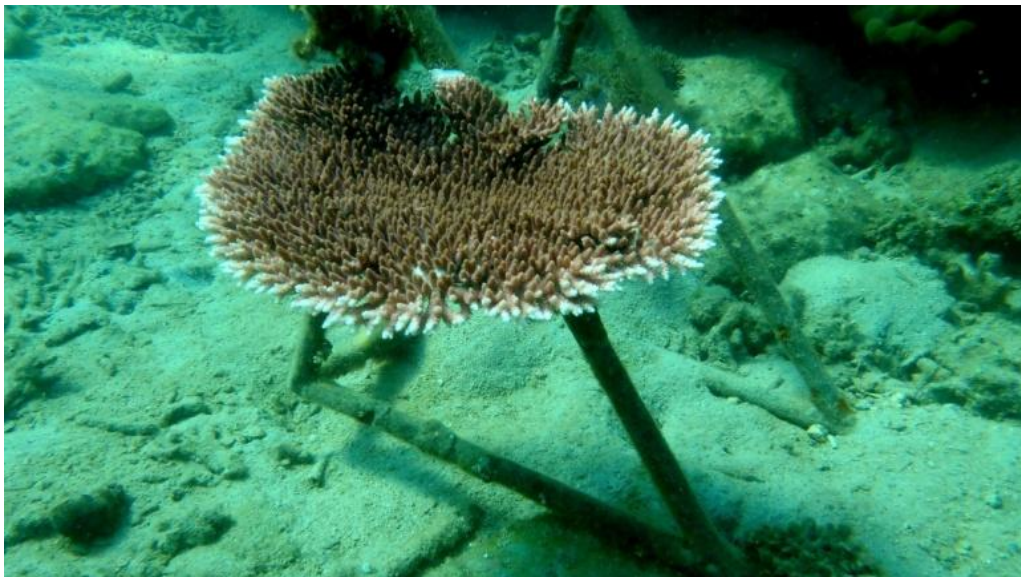


Fig. 31. Real coral on a metallic construction (Pulau Kapas).



Fig. 32. Artificial coral reefs (Pulau Kapas).

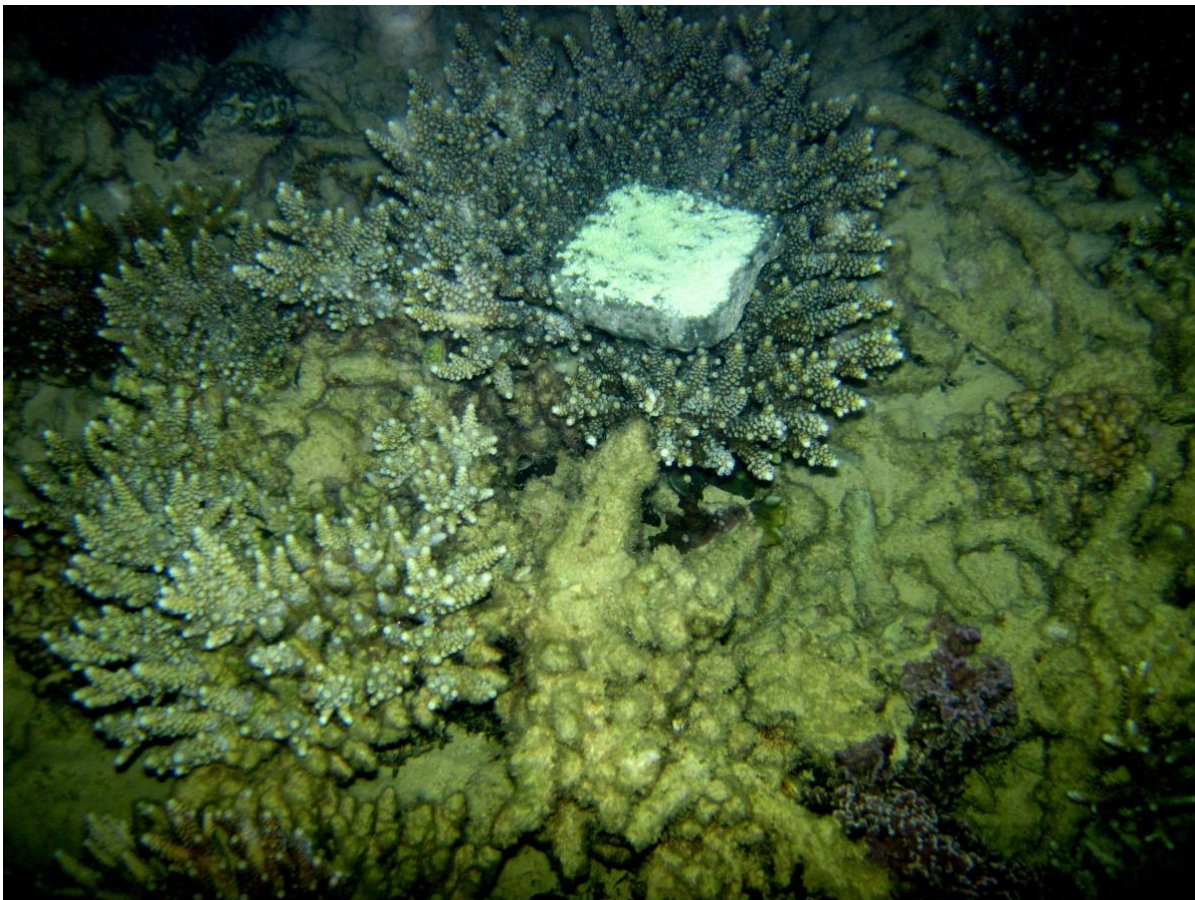


Fig. 33. An artificial luminescent block inside real corals.

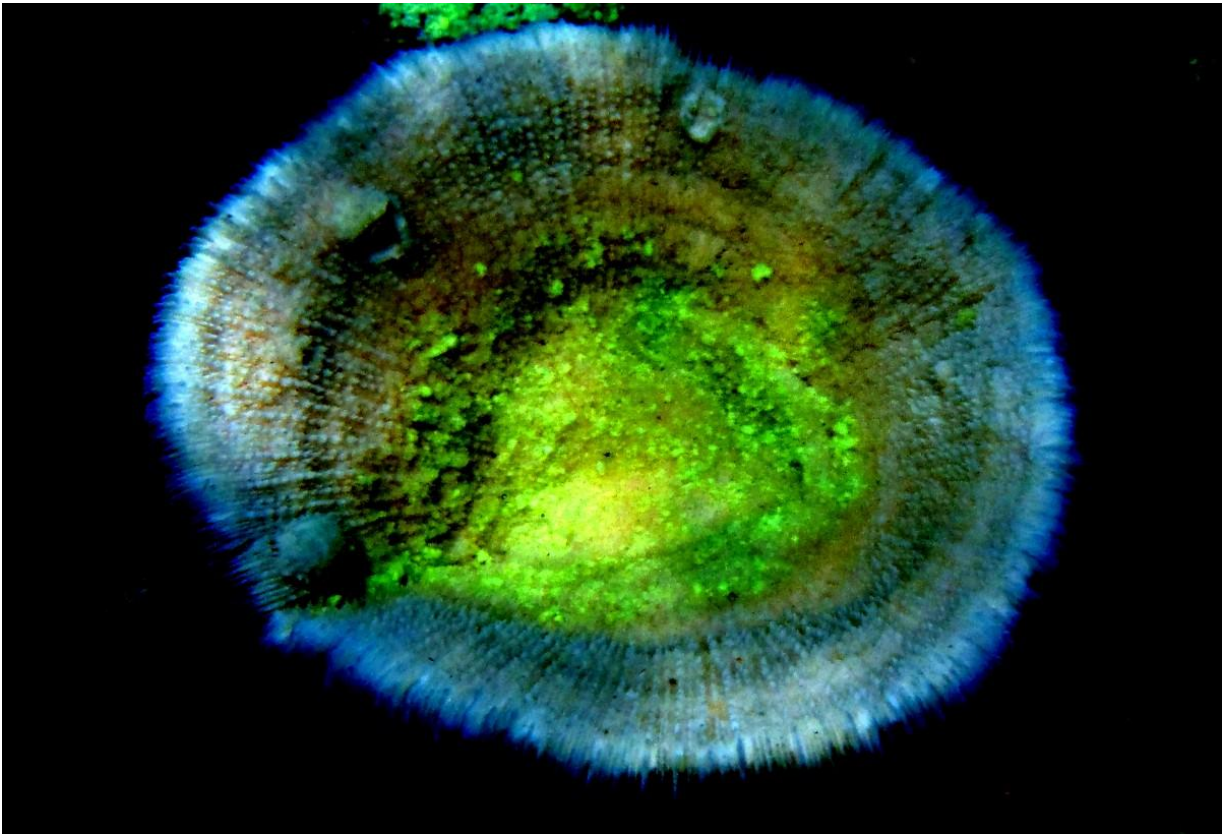


Fig. 34. Night luminescence of a real coral covered with a phosphor.

5. Conclusions

Short review is given to show the past and present of luminescent materials. Single-phase SrAl_2O_4 and multiphase $\{\text{SrAl}_2\text{O}_4+\text{Sr}_4\text{Al}_{14}\text{O}_{25}\}:\text{Eu}^{2+}$ doped phosphors have been synthesized by SSR and the combustion method. The CCL-SEM express analysis has been used to study the structure, morphology, and distribution of emission centers over the specimen surface at a high spatial resolution of about $2\ \mu\text{m}$. Two mixed phases - $\text{Sr}_4\text{Al}_{14}\text{O}_{25}$ with emission peaking at 490 nm and SrAl_2O_4 with emission peaking at 520 nm have been detected and their surface distribution in multiphase phosphors synthesized using SSR has been demonstrated. A single phase of SrAl_2O_4 has been detected in specimens synthesized by the combustion method. The emission of defects in the blue spectral region and Eu^{3+} ions in the red spectral region has been observed using CCL analysis as well. The images recorded in combined CCL and SE modes have shown both the fine structure and luminescence color information in the studied phosphors. Therefore, the local CCL method has made it possible to identify areas with different phases, heterogeneous doping, impurities, and defects. It is a good supplement to the quantitative integral PL spectra interpretation.

The UV excited $\text{SrAl}_2\text{O}_4:\text{Eu}$ (1%) crystal has shown two emission bands in the green (520 nm) and blue regions (450 nm) at low temperatures. A green pc-LED has been prepared

with a 365-nm UV InGaN chip. The CIE chromaticity diagram has confirmed that the prepared pc-LED emits bright green light with good color coordinates ($x = 0.288$, $y = 0.47$).

For the first time, experiments with an artificial stone covered with $\text{SrAl}_2\text{O}_4:\text{Eu}^{2+},\text{Dy}^{3+}$ based phosphor have been conducted under real sea conditions in Pulay Payar Marine Park Malaysia. Strong and bright blue-green (turquoise) luminescence has been observed and registered under water.

References

- [1] J. Holsa, *Electrochem. Soc. Interface* 18 (4), 42 (2009).
- [2] K. Van den Eeckhout, P.F. Smet, and D. Poelman, *Materials* 3, 2536 (2010).
- [3] P. F. Smet, D. Poelman, and M. P. Hehlen, *Opt. Mater. Express* 2, 452 (2012).
- [4] H.F. Brito, M.C.F.C. Felinto, J. Hölsä, T. Laamanen, M. Lastusaari, M. Malkamäki, P. Novák, L.C.V. Rodrigues, and R. Stefani, *Opt. Mater. Express* 2, 420 (2012).
- [5] L.C.V. Rodrigues, H.F. Brito, J. Holsa, and M. Lastusaari, *Opt. Mater. Express* 2, 382 (2012).
- [6] T. Aitasalo, J. Holsa, J. Krupa, M. Lastusaari, J. Niitykoski, in: J. Krupa, N. Kulagin (Eds.), *Physics of Laser Crystals*, Kluwer Academic Publisher, Netherlands, 2003.
- [7] H. Chander, *A Review on Synthesis of Nanophosphors-Future Luminescent Materials*, *Material Science and Engineering*, R49, 113, 2005.
- [8] C. Feldmann, T. Jüstel, C.R. Ronda, and P.J. Schmidt, *Adv. Funct. Mater.* 13, 511 (2003).
- [9] J. Botterman, J. J. Joos, and P. F. Smet, *Phys. Rev. B* 90, 085147 (2014).
- [10] D. Dutczak, T. Jüstel, C. Ronda, and A. Meijerink, *Phys. Chem. Chem. Phys.* 17, 15236 (2015).
- [11] M. Nazarov, M. G. Brik, D. Spassky, and B. Tsukerblat, *J. Lumin.* 182, 79 (2017).
- [12] J. Hölsä, *Electrochem. Soc. Interface* 18, 42 (2009).
- [13] M. Born, T. Justel, *Chem. Unserer Zeit.* 40, 294 (2006).
- [14] M. Nazarov, S. Mammadova, D. Spassky, S. Vielhauer, S. Abdullayeva, A. Huseynov, and R. Jabbarov, *Opt. Mater.* 75, 448 (2018).
- [15] S. K. Obyden, G. V. Saparin, and G. V. Spivak, *SCANNING*, 3, 181 (1980).
- [16] G. V. Saparin and S. K. Obyden. *SCANNING* 10, 87 (1988).
- [17] S.K. Obyden, P.V. Ivannikov, and G. V. Saparin. *SCANNING* 19, 533 (1997).
- [18] M. Nazarov, P. Ivannikov, and D. Spassky *J. Surf. Invest.: X-Ray, Synchrotron Neutron Tech.* 13, 1020 (2019).
- [19] G. Blasse and B. C. Grabmeyer, *Luminescent Materials*, Springer-Verlag, Berlin, 1994.
- [20] F. C. Palilla, A. K. Levine, and M. R. Tomkus, *J. Electrochem. Soc.* 115, 642 (1968).
- [21] S. H. M. Poort, W.P. Blockpoel, and G. Blasse, *Chem. Mater.* 7, 1547 (1995).
- [22] F. Clabau, X. Rocquefelte, S. Jobic, P. Deniard, M. H. Whangbo, A. Garcia, and T. Le Mercier, *Chem. Mater.* 17, 3904 (2005).
- [23] J. Holsa, T. Laamanen, M. Lastusaari, J. Niitykoski, and P. Novak, *J. Rare Earths* 27, 550 (2009).

- [24] M. Nazarov, M.G. Brik, D. Spassky, B. Tsukerblat, A. Nor Nazida, and M. N. Ahmad-Fauzi, *J. Alloy Compd.* 573, 6 (2013).
- [25] M. Nazarov, A. Nor Nazida, M. N. Ahmad-Fauzi, and P. Ivannikov, *Microsc. Anal.* 27, 13 (2013)
- [26] M. Nazarov, A. Nor Nazida, M. N. Ahmad-Fauzi, A. Badri Ismail, and P. Ivannikov, *J. Mold. Phys Sci.* 11, 147 (2012)
- [27] M. Kamada, J. Murakami, and N. Ohno, *J. Lumin.* 87–89, 1042 (2000).